Start-up runaway generation with neutral and low Z impurity reduced screening effects at the KSTAR Ohmic plasma

Y. Lee[1,2], P.C. de Vries[2], P. Aleynikov[3], J. Lee[4], Y.-S. Lee[4], H.-T. Kim[5] and Y.-S. Na[1*]
[1] *Department of Nuclear Engineering, Seoul National University, Seoul, South Korea*
[2] *ITER Organization, Route de Vinon sur Verdon, CS 90 046, 13067 St Paul Lez Durance, France*
[3] *Max-Planck Institute fur Plasmaphysik, Greifswald, Germany*
[4] *Korean Institute of Fusion Energy, Daejeon, South Korea*
[5] *Culhan Centre of Fusion Energy, Culham Science Centre, Abindon OX14 3DB, United Kingdom of Great Britain and northern Ireland*

1. Introduction

While physics of Runaway Electrons (REs) is a branch of tokamak research recently focusing on investigating, suppressing and mitigating it in disruption phase, there has been less attention given to generation of the REs during start-up phase after an early tokamak start-up study established. A recent ITER plasma initiation revision [1] indicated that ITER plasmas have a risk of producing the REs due to low prefill gas pressure, required for the plasma burn-through, and consequently low density during the plasma initiation. To ensure plasma initiation in ITER, it is necessary to avoid runaway dominant start-up, where runaway current dominates thermal current, prohibiting thermal population from burning [2]. Questions arise, how to avoid or mitigate formation of the REs during the ITER start-up, and do we understand all facts of the start-up REs generation, especially, when we interpret it with many of mechanisms derived assuming the fully ionized plasmas and Maxwellian distribution for the thermal electrons. In this work, we will study the Primary generation of the REs in the KSTAR by employing the DYON [4] and the Fokker-Planck solver [3] adjusted to the start-up phase with generalized collision operator reliable at the start-up REs study. There is no avalanche mechanism or transport loss of the REs in consideration.

In the start-up REs study, a reduced screening effect can be important due to neutral before the plasmas formed or due to impurity when Plasma Surface Interaction (PSI) like sputtering happens. This effect can affect speeding-up process of non-runaway electrons from low energy to critical energy and therefore a model of the reduced screening effect should be reliable in this energy range. However, an evaluation of the reduced screening effect on electron-ion elastic and electron-electron inelastic collision has typically concentrated on high Z impurities with plasma parameters relevant to post-disruption phase to examine slowing-down process of the REs because the REs mitigation strategy employs Ne and Ar [5-7]. On the other hand, for the start-up REs study, we should describe speeding-up process of the electrons accounting for the reduced screening effect at low incident electron energy on the neutral and with the plasma parameters and impurity species different from the post-disruption phase. This paper will introduce a stopping power model for the electron energy with the low incident energy on the hydrogen, analyse a total reduced screening effect with various ionization fractions and revisit the reduced screening effect by low Z impurity when the PSI effect is significant.

2. Bifurcation of start-up REs generation observed in KSTAR experiment

The KSTAR has a similar operation window to the ITER. During 2020 campaign in the KSTAR, there were 25 successful discharges with the pure Ohmic start-up. There were two main signs of the REs. ECE signal skyrocketing implies REs formation and HXR intensity does REs loss. We classified the discharges as groups A and B. There are 9 discharges in the group A with the strong signs of the REs. There are 16 discharges in the group B with the weak signs of the REs. In Fig. 1a, a discharge 26031 in the group A shows the ECE signal and the HXR intensity higher than a discharge 26696 in the group B. Breakdown condition does not matter (Fig. 1b) but bifurcation of the two groups happens at t = 0.2 s, which suggests that it is important to understand early development of the REs (Fig 1c).

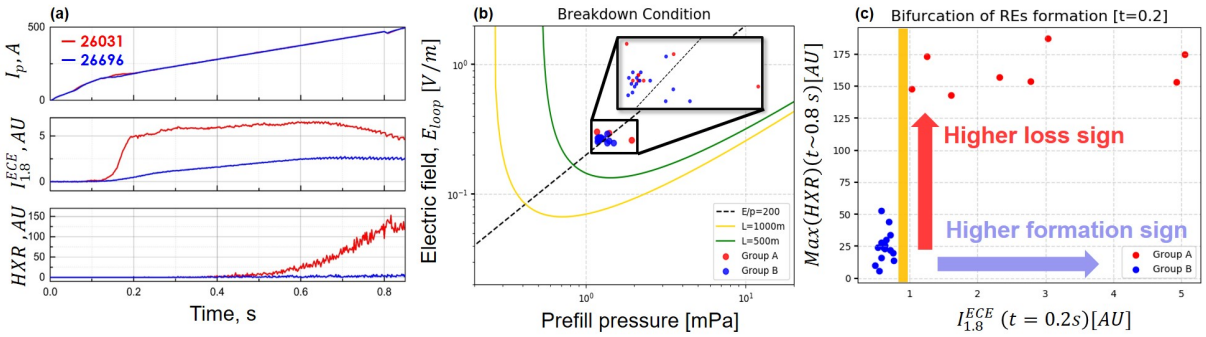

Figure 1. *(a) time evolutions of the plasma current (I_p), the ECE signal ($I_{1.8}^{ECE}$) and the HXR intensity of the discharge 26031 (red) and the discharge 26696 (blue), (b) a scatter plot of the breakdown condition of the group A (red) and the group B (blue), (c) a scatter plot of the maximum HXR intensity during the start-up against the ECE signal at t = 0.2 s of the group A (red) and the group B (blue).*

3. Generalized collision operator for start-up REs modelling

We took collisional integral for collision with free electrons in a form of [11] with Coulomb logarithms from [6], taking into account ionization potentials modified [12] due to increased temperature. As collisional integral for collision with bound electrons, we adopted a low T_e asymptote of the collisional integral on the free electrons consistent with the Bethe model [6]. We extended the Bethe model for the electrons on hydrogen, accounting for the reduced screening effect on the inelastic collision at low incident electron energy. Except for hydrogen, we extrapolated the Bethe model.

For the electrons with the low incident energy, we introduced the BEBED stopping power on the hydrogen atom adopting the BE scaling method for excitation from 1s->2p transition to 1s->10p transition [8] and the Binary-Encounter-Dipole (BED) model for ionization using the ionization stopping cross section [9].

$$\sigma_{\mathrm{sti,BED}} \equiv B \int_0^{(t-1)2} (w+1)\left(\frac{d\sigma}{dw}\right)_{BED} dw$$

$$\mathrm{W_{BEBED}} \equiv \sum_{n=2}^{10} n_H v \sigma_{ex,BE}^{1s\to np}(\Delta E)^{1s\to np} + n_H v \sigma_{sti,BED}$$

We splined the BEBED model and the Bethe model, and named the splined model the Bethe-BEBED model. We introduced the total reduced screening effect considering the total number of free electrons and that of bound electrons.

$$\frac{\tilde{\nu}_S^{ee}}{\tilde{\nu}_{S,CS}^{ee}} = \frac{W_{free} + W_{bound}}{W_{free}}$$

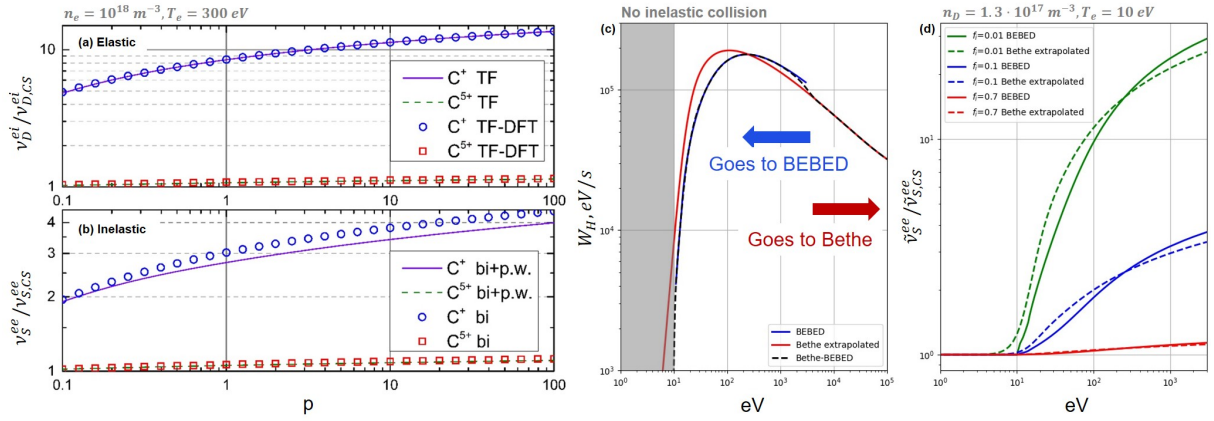

Figure 2. *(a) the reduced screening effect on the elastic collision by partially stripped carbon ions (solid violate line for C^+ with the TF model, dashed green line for C^{5+} with the TF model, blue circle marker for C^+ with the TF-DFT model and red square marker for C^{5+} with the TF-DFT model), (b) the reduced screening effect on the inelastic collision by the partially stripped carbon ions (solid violate line for C^+ with the plasma wave excitation effect, dashed green line for C^{5+} with the plasma wave excitation effect, blue circle marker for C^+ without the plasma wave excitation effect and red square marker for C^{5+} without the plasma wave excitation effect), (c) the stopping powers for the electrons on the hydrogen atom with $n_H = 1.3 \cdot 10^{17} m^{-3}$ and (d) the total reduced screening effect on the inelastic collision with various ionization fractions (f_i = 0.01 (green), 0.1 (blue) and 0.7 (red)) and the two models (the BEBED model (solid) and the Bethe model extrapolated (dashed)).*

As seen in Fig. 2a, the Thomas-Fermi model [6] is consistent with the TF-DFT model [7] at the start-up phase. Fig. 2b shows that neglecting the plasma wave excitation due to the long-range Coulomb interaction can overestimate the reduced screening effect about 10% at the start-up phase. In the Fokker-Planck solver, the slowing down frequency of the free electrons has the effect of the plasma wave excitation [6]. Fig. 2c illustrates that the Bethe-BEBED model, implemented in the Fokker-Planck solver, follows the BEBED model with the low incident energy and the Bethe model with the high incident energy. As depicted in Fig. 1d, shapes of the two models of the total reduced screening effect by the deuterium atoms with various ionization fractions (0.01, 0.1 and 0.7) are different. Below the minimum energy required for the inelastic collisions, which is 10.2 eV for the 1s->2p transition, the total reduced screening effect with the BEBED model is unity while that with the Bethe model extrapolated isn't. As the ionization fraction increases, the total reduced screening effect decreases due to increased friction force by the free electrons.

4. Numerical workflow

We employed the DYON [4] without an electromagnetic effect and the Fokker-Planck solver [3] adjusted to the start-up phase. The DYON gives plasma parameters (e.g. the electron density, the electron temperature, the resistive electric field and the density of impurities) required for the Fokker-Planck solver, which provides an evolving distribution on 2D momentum space. We computed the Primary generation rate at a critical gamma [10] by identifying a saddle point in phase space with the generalized collision operator in the section 3.

5. Two stages of the Primary generation and roles of neutral and impurity

We investigated a discharge 12328 as a standard Ohmic scenario in the KSTAR. As seen in Figs 3a and 3d, there is the Primary generation during the breakdown. The deuterium neutral at this stage has a role of kinetically suppressing the REs generation rate, featured as a difference between the steady-state calculation and the analytic formula [5] modified as being consistent with the generalized collision operator in the section 3. The global closed flux surface formed at 45 ms, suggesting there be no REs seed population confined by the global closed flux surface.

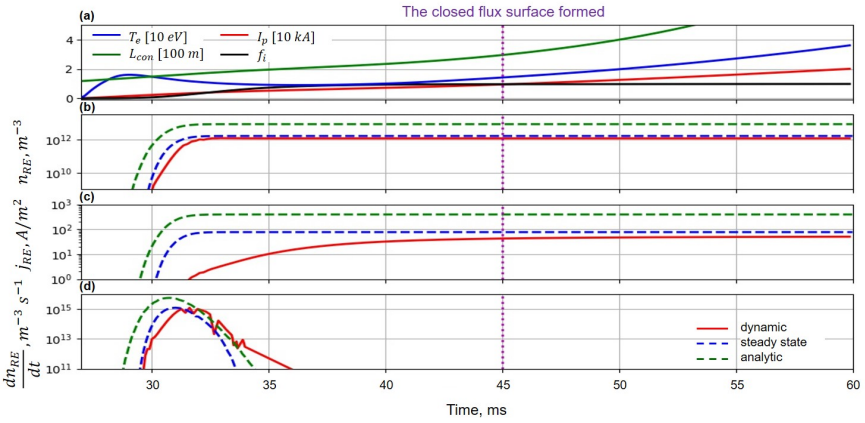

Figure 3. *(a) temporal evolutions of the electron temperature (T_e), the plasma current (I_p), the connection length (L_{con}) and the ionization fraction (f_i) from the DYON, (b) the density of the REs (n_{RE}), (c) the current density of the REs (j_{RE}) and (d) the Primary generation rate ($\frac{dn_{RE}}{dt}$) with the dynamic calculation (solid red line), the steady-state calculation (dashed blue line) and the analytic formula (dashed green line). Dotted violate line represents the formation of the global flux surface.*

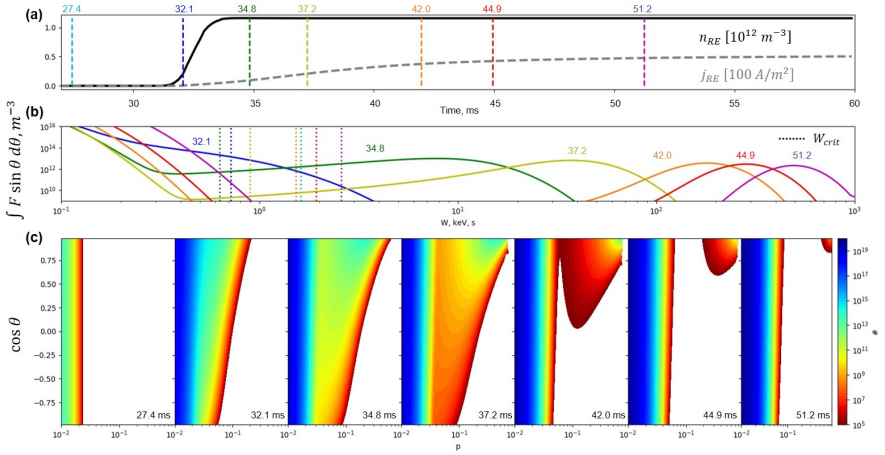

Figure 4. *(a) temporal evolutions of the REs density (n_{RE}) and the REs current density (j_{RE}), (b) isotropic parts of the distribution F with the critical kinetic energy of the REs (W_{crit}) (dotted line) and (c) 2D contour snapshots of the evolving distribution. All colors in (a) and (b) except black and gray correspond to time.*

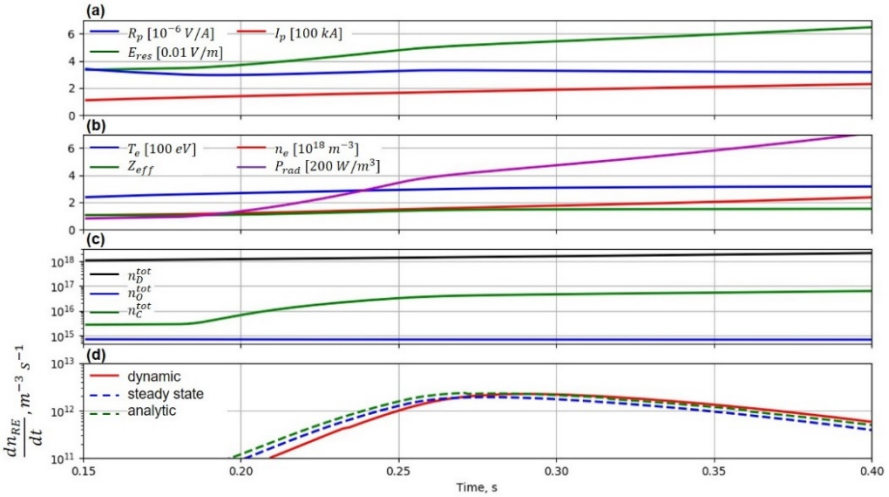

Figure 5. *(a) temporal evolutions of the plasma current (I_p), the resistive electric field (E_{res}) and the Spitzer resistivity (R_p), (b) temporal evolutions of the electron temperature (T_e), the electron density (n_e), the effective charge (Z_{eff}) and the radiative power (P_{rad}), (c) temporal evolutions of the total density of the deuterium species (n_D^{tot}), of the oxygen species (n_O^{tot}) and of the carbon species (n_C^{tot}) from the DYON, (d) temporal evolutions of the Primary generation rates ($\frac{dn_{RE}}{dt}$) with the dynamic calculation (solid red line), the steady-state calculation (dashed blue line) and the analytic formula (dashed green line).*

Taking into account the possibility of local confinement before the global closed flux surface formed, we analysed evolutions of a distribution (Fig. 4). As the breakdown happens (t = 32.1 ms), an isotropic part of tail population, supplied from bulk, increases (Fig. 4b). At t = 34.8 ms near end of the breakdown, the electric field pulled out front of the tail with high energy while back of the tail with intermediate energy dropped (Fig. 4b). The tendency maintained and the Dreicer mechanism terminated, accounting for the increasing current carried by the

REs (Fig. 4a) and the decreasing Primary generation rate (Fig. 3d). The tail population had high directionality and eventually formed a beam-like distribution (Fig. 4c).

Another event when there is the Dreicer flow is the PSI due to the sputtering of the carbon impurity (Fig. 5c, d), which has an indirect role of driving the REs generation at this stage. As the carbon penetrates into the plasmas, a rise in the electron temperature becomes slower due to the enhanced radiative power and the effective charge increases (Fig. 5b), which results in a delay of decrease in the Spitzer resistivity (Fig. 5a). The plasma current has a fixed rate and thus the resistive electric field increases, driving the REs generation (Fig. 5a, d).

6. Discussion

There is good agreement with the dynamic calculation of the REs density during the breakdown against the steady-state calculation (Fig. 3b). The runaway current, meanwhile, has disagreement because it takes time for the runaway electrons to reach the relativistic region, ignored in the steady-state calculation (Fig. 3c). Nevertheless, the result supports using the fluid description for the start-up REs analysis with the steady-state calculation because the effect of the runaway current is negligible compared to the thermal current (Fig. 3a, c). Moreover, usage of the analytic formula, which has little difference from the steady-state calculation, is even reasonable for the fluid modelling of the REs during the PSI stage (Fig. 5d).

There are the two stages of the Primary generation. To determine which stage has a key role in bifurcating the two groups introduced at the section 2, the kinetic solver should include the avalanche mechanism even with the REs transport. If the Primary generation driven by the impurity has a key role, it is good news to the ITER because the ITER has the beryllium wall.

7. Conclusion

This paper investigated the start-up REs generation in the KSTAR with the kinetic model because the neutral or the impurity can kinetically affect the speeding-up process of the REs. The first stage of the Primary generation was the breakdown stage where the neutral kinetically hinders the fast electrons from developing. The second stage of the Primary generation was the PSI phase where the impurity indirectly drives the REs generation. In both stages, the kinetic description of the REs generation had little difference with the fluid description, the steady-state calculation for the breakdown stage and even the analytic formula for the PSI stage, which can provide justification for using the fluid description for the Primary generation when modelling the start-up REs at the KSTAR with a plasma burn-through code (e.g. the DYON).

This research was supported by R&D Program of "R&D on Key Technology of ITER Components – Study on start-up supra-thermals/runaways for ITER plasmas operation (code No. R&D-IN2022-11)" through the Korea Institute of Fusion Energy (KFE) funded by the Government funds, Republic of Korea.

Disclaimer: ITER is a Nuclear Facility INB-174. The views and opinions expressed herein do not necessarily reflect those of the ITER Organization.

8. Reference

[1] de Vries P.C. and Gribov Y. 2019 ITER breakdown and plasma initiation revisited *Nucl. Fusion* **59** 096043
[2] de Vries P.C. *et al* 2020 Analysis of runaway electron discharge during Joint European Torus plasma start-up *Plasma Phys. Control. Fusion* **62** 125014
[3] Aleynikov P. and Breizman B.N. 2017 Generation of runaway electrons during the thermal quench in tokamaks *Nucl. Fusion* **57** 046009
[4] Hyun-Tae K. *et al* 2012 Enhancement of plasma burn-through simulation and validation in JET *Nucl. Fusion* **52** 103016
[5] Martin-Solis J.R. *et al* 2017 Formation and termination of runaway beams in ITER disruptions *Nucl. Fusion* **57** 066025
[6] Breizman B.N. *et al* 2019 Physics of runaway electrons in tokamaks *Nucl. Fusion* **59** 083001
[7] Hesslow L. *et al* 2017 Effect of Partially Screened Nuclei on Fast-Electron Dynamics *Phys. Rev.* **118** 255001
[8] Yong-Ki K. 2001 Scaling of plane-wave Born cross sections for electron-impact excitation of neutral atoms *Phys. Rev. A.* **64** 032713
[9] Yong-Ki K. and Eugene M.R. 1994 Binary-encounter-dipole model for electron-impact ionization *Phys. Rev. A.* **50** 3954
[10] Martin-Solis J.R., Loarte A. and Lehnen M. 2015 Runaway electron dynamics in tokamak plasmas with high impurity content *Phys. Plasmas* **22** 092512
[11] Papp G., Drevlak M., Fulop T. and Helander P. 2011 Runaway electron drift orbits in magnetostatic perturbed fields *Nucl. Fusion* **51** 043004
[12] Sauer S.P., Sabin J.R. and Oddershede J. 2018 Z-dependence of mean excitation energies for second and third row atoms and their ions *J. Chem. Phys.* **148** 174307